X Encontro Brasileiro sobre Adsorção
27 a 30 de Abril de 2014
Guarujá - SP

SYNTHESIS OF NIOBIUM MICRO-MESOSTRUCTURED MATERIALS USING ALKYLAMMONIUM CATIONS.

D.C. Mazarin[2]; R. Fernández-Felisbino[1]; D. Cardoso[2]; E. L. Gomes[1]

1- Universidade Federal de São Paulo, DCET, Setor de Eng. Química. R. Prof. Artur Riedel, 275 - Jd. Eldorado - Diadema - SP – Brazil - 09972-270. Phone: +55(11) 3319-3300 – Fax: +55(11) 4043-6428 – Email: eliezer.ladeia@unifesp.br
2- Universidade Federal de São Carlos, Depto. Engenharia Química. Campus São Carlos, Rod. Washington Luís, km 235 - São Carlos - São Paulo – Brazil – 13565-905. Phone:+55(16) 3351-8111 – Fax: +55 (16) 3361-2081

ABSTRACT: Due to the great scientific and industrial interest in oxidation reactions of organic compounds, the aim of this work was the synthesis and analysis of niobium containing micro-mesostructured materials. The molecular sieve Nb-MCM-41 was modified based on their property of ion exchange: four different alkylammonium cations (tetramethylammonium, tetraethylammonium, tetrapropylammonium and tetrabutylammonium), each in its turn, were "anchored" in the mesoporous walls and provided the templating of the microstructures. After ion exchange, the reaction mixtures were submitted to the thermal treatment followed by careful calcination, producing the niobium containing micro-mesostructure. These materials were characterized by X-ray diffraction, nitrogen physisorption and other techniques.

KEYWORDS: niobium micro-mesostructures; MCM-41; ion exchange; alkylammonium cations; nanostructures.

1. INTRODUCTION

The hierarchically structured porous materials are of great interest for catalysis, since the precise control of the porous structure on different scales can help reduce or control the mass transport limitations within the catalyst (Coppens et al., 2001).

Most of the microporous molecular sieves is synthesized using organic templates. A template has the property to assembly itself to the fundamental building blocks that will build the molecular sieve, driving the crystallization to the final desired structure. Generally, the zeolitic structure that better stabilizes itself with certain template will be preferentially formed during the synthesis (Burchart et al., 1997).

Some known examples are the synthesis of the MFI structure using tetrapropylammonium hydroxide (TPAOH) (Gualtieri et al., 2006), the MEL structure that is typically produced using tetrabuthylammonium hydroxide (TBAOH) (Burchart et al., 1997), tetraethylammonium hydroxide (TEAOH) that is used for the synthesis of BEA and MTW structures (Gopal et al., 2001; Pusparatu et al., 2012). Some papers have shown the use of tetramethylammonium hydroxide (TMAOH) for the alternative synthesis of sodalite zeolite without the addition of alkaline cations (Jafari et al., 2013). It is known that the presence of TMA^+ cation is important as co-template for the formation of the building blocks of mesoporous sieves of MCM type, reducing significantly its synthesis time (Cheng et al., 1997).

Due to the weak acidity and low hydrothermal stability of the mesoporous sieve MCM-41, there is still no application for this material in industrial processes. However, its synthesis is simple and allows for excellent control of the size of its mesopores (Beck et al., 1992; Wang et al., 2011). Additionally, this molecular sieve allows the access of large molecules to its channels. The motivation for the research on the synthesis of micro-mesostructured materials is based on the following aspects (On et al., 2001):

I) the necessity of development of efficient catalysts with pores in the range of mesopores;

II) the mesoporous catalysts do not have

short range ordering and, from this point of view, they are more similar to the amorphous materials than the crystalline ones;

III) combine the advantages of the microporous sieves and mesoporous materials in only one composite material.

In this context the micro-mesostructured materials come as an interesting solution as they combine the properties of both types of molecular sieves. We can generate, by controlling the synthesis process, a MCM-41 based structure that has better thermal and hydrothermal stability as well as strong catalytic activity, by recrystallization of their mesoporous walls with basic zeolitic structures.

Kloetstra et al. (1997) have synthesized MFI/Al-MCM-41 and MFI/Al-HMS composites using a method named "ion exchange method". The synthesis of these composites is based on the ion exchange of the compensation cations of the structure by the tetrapropylammonium cations (TPA^+), which are positioned on the surface of the MCM-41 mesopores. During the recrystallization process these cations induce the formation of zeolitic nuclei on the walls of the pores of MCM-41 via heterogeneous nucleation.

Thus, the aim of this work was to synthesize micro-mesostructured composite materials from a Nb-MCM-41 matrix, carrying out the ion exchange and recrystallization procedures as described by Kloetstra et al. (1997), using the following alkylammonium cations as templates for the nucleation of zeolitic structures on the pores walls: TMA^+, TEA^+, TPA^+ and TBA^+.

2. EXPERIMENTAL

2.1. Synthesis of Nb-MCM-41 matrix

The synthesis procedure is based on the method proposed by Cai et al. (1999). The compositon of the reactional mixture was: 1 SiO_2 : 0,01 Nb_2O_5: 0,15 CTABr: 19,5 NH_3: 82,5 H_2O. First, CTABr (cetyltrimethylammonium bromide, Aldrich, 98%) was dissolved under stirring in water at 60 ºC for 1 hour and, after cooling, it was added the ammonium hydroxide solution (Cinética Química, 25% w/w). Tetraethyl orthosilicate (TEOS, Aldrich, 99%) was added and immediately it was dropped the acid heptafluorniobic solution (H_2NbF_7 , 5%m/m, prepared by the digestion of Nb_2O_5, CBMM, HY340, with hydrofluoric acid). The mixture was sealed and allowed the aging at room temperature for 24 hours. The thermal treatment was carried out in teflon-lined stainless-steel autoclaves under autogenous pressure at 100 ºC for 72 hours. Then the solution was filtered, washed with deionized water and dried at 110 ºC for 24 hours. This material was named as **M** (Nb-MCM-41 matrix, as synthesized). The surfactant occluded was removed by calcination in N_2 (2 hours) and synthetic air (6 hours) at 540 ºC (**MC**, Nb-MCM-41 matrix, calcined).

2.2. Synthesis of niobium containing micro-mesostructured materials

The solutions for cation exchange were prepared with their respective hydroxides sources (Aldrich): $TMAOH.5H_2O$ (≥ 97%), TEAOH sol. (35% m/m), TPAOH sol. (1 $mol.L^{-1}$), TBAOH sol. (1 $mol.L^{-1}$). The concentration of the solutions for cation exchange was $2{,}5x10^{-2}$ $mol.L^{-1}$ and used in the proportion of 1:10 (g Nb-MCM-41 calcined / g sol.). The cation exchange was carried out at RT for 24 hours. These materials were named as **TX**, where **X** is the number of carbons in the alkyl cation (1 to 4). The recrystallization was performed using glycerol (Baker, 13% H_2O w/w) as solvent in autoclaves (120 ºC, 24 h). The recrystallized materials were named as **RX** (**X** with the same meaning). The solids obtained were carefully calcined under N_2 flow at a heating rate of 5 °C/min from RT to 150 °C, kept at this temperature for 1 h, followed by a heating rate of 1 °C/min up to 420 °C, when the flow was changed to synthetic air (420 ºC for 10 h). These materials were named **RXC**, (**C** = calcined).

2.3. Characterization

The XRD measurements were performed on a Siemens D-500 diffractometer using Cu-Kα radiation at 40 kV and 40 mA. Diffraction data were recorded at an interval of 0.02 and scanning speed of 0.6º / min in the range of 1 to 10º.

N_2 physisorption isotherms were obtained at 77 K using a Nova-1200 analyzer (Quantachrome Co.). Before measurements, the samples were outgassed at 423 K for 2 h.

TEM images of the samples were obtained on a Philips CM-120 transmission electron microscope at 120 kV. SEM images of the samples were obtained on a Philips XL30-FEG scanning electron microscope operating at 30 kV.

Coordination environment of Nb species was determined by DRUV-vis spectroscopy. The

measurement was performed at room temperature using a Varian Cary 5 in the wavelength range of $200 < \lambda < 400$ nm. The spectra were obtained for a constant mass in the probe (1 g) and the data transformed to Kubelka-Munk.

Thermogravimetric analysis (TA/TG/DTG) were performed with a thermobalance Therma Analyst 2100 (TA Instruments), using 10 mg of solid. The samples were heated under synthetic air flow, from 25 to 1000 ºC and rate of 10 ºC/ min.

3. RESULTS AND DISCUSSION

In Figure 1 the XRD patterns of samples M, MC, T3, R and R3C are presented. The peaks for the samples M and MC are characteristic of MCM-41 mesoporous materials (Gomes, 2005). There are at least 3 diffraction peaks, thus showing that the as synthesized and calcined materials have good organization. The matrix (M) shows peaks with lower intensity compared to the calcined sample (MC) due to the presence of the surfactant occluded in its mesopores. The presence of Nb does not interfere in the formation of mesophase.

After the ion exchange the sample T3 presented diffraction peaks that remained practically unchanged in their number, intensities, height at half maximum and positions, relative to the calcined sample (MC). The ion exchange process did not modify the hexagonal structure, because the low concentration of the organic cation (in this case, TPAOH, 2.5×10^{-2} mol.L^{-1}), and consequently of OH^-, was not sufficient to dissolve the pore wall of Nb-MCM-41 calcined. Apparently there was a slightly shift of the peak (100) to smaller angles, which means that the interplanar spacing d_{100} in this sample increased a little with respect to the sample MC.

We can also observe that the XRD patterns, concerning to the samples R3 and R3C, presented only the main peak (100), and the other ones, related to the secondary plans, disappeared. We can say that the hexagonal arrangement was maintained, but it is not so well aligned as before. The intensity of this peak for the sample R3 diminished and this means that possibly part of the pore walls were consumed during the recrystallization process, leading to a partial collapse of the structure. If this treatment were more intense (higher temperature, long time), the hexagonal system would be completely dismounted. Finally, the sample R3C presented a better organization related to its precursor. Possibly, when the organics were removed, the walls could be restructured in some extension.

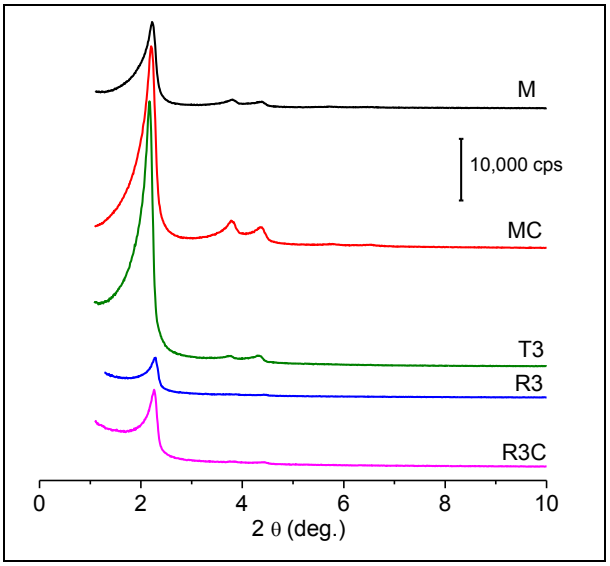

Figure 1. X-Ray diffractograms for the samples in the process to produce the composite R3C.

The behavior for the other process with TMA^+, TEA^+ and TBA^+ cations were very similar to the process described here. The Table 1 present the parameters obtained from the diffractograms of the samples in this work.

Table 1. Textural parameters of the samples for all steps of preparation of the composite.

Sample	OD [a] (%)	FWHM [b] (º)	d_{100} [c] (Å)	a_H [d] (Å)
M	36	0.26	40	46
MC	95	0.29	40	46
T1	66	0.33	39	45
R1	3	0.18	41	47
R1C	5	0.18	39	45
T2	95	0.27	40	46
R2	7	0.19	38	44
R2C	10	0.20	39	46
T3	100	0.23	41	47
R3	9	0.20	39	45
R3C	18	0.20	39	45
T4	40	0.26	40	47
R4	11	0.26	41	46
R4C	6	0.22	41	47

[a] Organization Degree = $(I_{100}/I_{100pattern})$x100; [b] Full Width at Half Maximum; [c] interplanar spacing of 100 planes; [d] hexagonal framework parameter

From this Table we observe that the

diminution of the organization degree during the recrystallization process is evidenced by the analysis of Tn and Rn steps. The low value of the organization degree does not mean that the material is poorly organized or the phase has colapsed, but when compared to the more organized sample (T3), this parameter becomes very low. Thus, the value of OD is not the ideal parameter to compare samples so different.

The FWHM parameter also depends on the intensity of peaks and varies between 0.18 and 0.33°. This parameter combined with OD gives us the real proportion of the organization of the mesoporous system. In general, the MC sample has the highest value of FWHM because it has the better organization among the samples, but we can see that the step of ion exchange also maintains a high value of FWHM, i.e., this process does not affect significantly the organization of the system.

The parameter a_H varies between 44 and 47 Å, a variation of only 3 Å (or an error of approximately 6%), what is in the range of expected error for different samples. Therefore, we can conclude that after the steps carried out to obtain the final composite material with a variety of organic cations, there is no significant modification of the structure of Nb-MCM-41 (sample M), but the reduction in intensity is related to a partial dissolution of the samples.

Figure 2 shows the XRD patterns of the samples RnC (final micro-mesostructured material). The diffraction peaks confirm the hexagonal phase, i.e., after the several steps for the preparation of the composite, the mesopores of MCM-41 were maintained. We can observe that the diffractograms of all samples retained the peak related to the plane (100), and the samples R3C and R4C presented the peaks related to the secondary plans. The sample R2C apparently also kept the secondary peaks , but only the plane (200) could be observed . The R1C sample did not show any secondary peak.

Regarding to the intensity of the peaks for these samples, we can say that the intensity of the peak (100) increase when there is an increasing in size of the chain of the exchange cation until TPA^+ and a decreasing to the sample that employed TBA^+. So, for this kind of synthesis, the micro-mesostructured material synthesized with the cation TPA^+ is better structured than the other exchange cations.

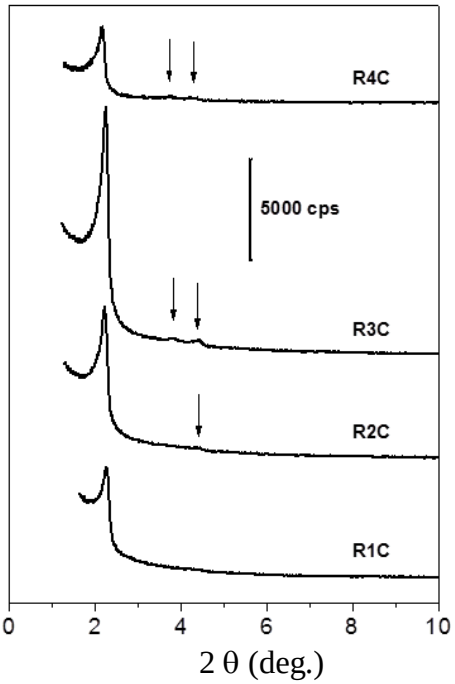

Figure 2. XRD patterns of the final micro-mesostructured material (RnC).

Figures 3 to 7 are micrographs (SEM) obtained for the as synthesized Nb-MCM-41 (sample M) and the final solid synthesized with TMA^+, TEA^+, TPA^+ and TBA^+ cations (R1C, R2C, R3C and R4C, respectively). In Figure 3 we can see that the morphology of the solid is not homogeneous, being composed of agglomerates of small particles (< 0.2 μm), agglomerates of large particles (≅1 μm) and solids with irregular shapes (> 5 μm). The larger agglomerates appear to be constituted of by intergrown particles that was formed due to the high solidification rate.

Possibly the variety of morphologies are related to the rapid nucleation and growth of solid, that even at room temperature can produce the MCM-41 (Bordoloi et al., 2006). Another aspect that can justify such behavior is that, despite the monomeric silica (TEOS) induces to solids with homogeneous morphology and dimensions for Si-MCM -41 (Occelli et al., 1999), the presence of Nb interferes with the formation and growth of these particles, modifying its kinetics of nucleation and growth, generating a variety of morphologies.

In Figures 4 to 7 we can see that, even after several treatments, the morphology obtained for the solids is very similar and, compared to the as synthesized Nb-MCM-41, little variation occurred, i.e. this process did not appreciably alter the morphology of the samples.

Figure 8 shows a micrograph (TEM) for the composite R3C and provides a view of the mesopores on direction [010]. There are well-formed and organized mesopores, confirming the XRD results, and showing that despite the steps of the process cited before, the mesoporous structure of Nb-MCM-41 matrix was maintained too. Beardlike structures can be also observed, as Huang et al. (2000) verified when synthesizing Al-MCM-41/MFI composite. These authors affirm that these structures arise from the partial structural collapse of mesophase during recrystallization.

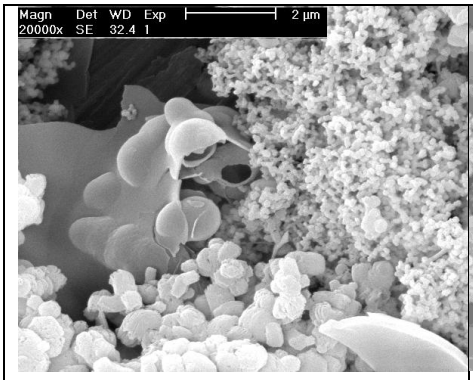

Figure 3. Sample as synthesized Nb-MCM-41 (M) (bar = 2 µm).

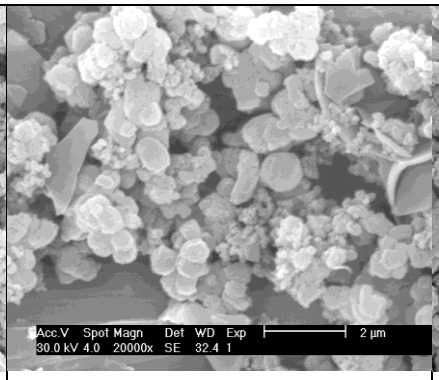

Figure 4. Micrograph of the sample R1C. (bar = 2 µm).

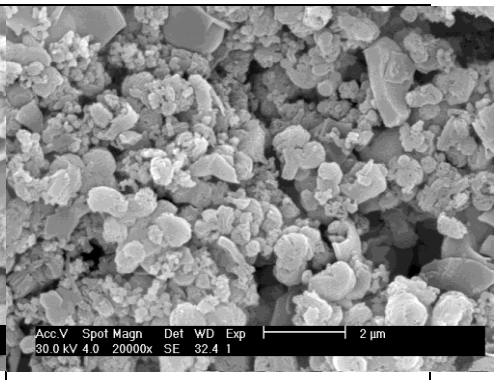

Figure 5. Micrograph of sample R2C. (bar = 2 µm).

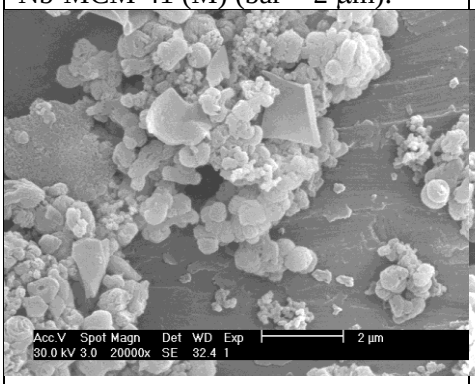

Figure 6. Micrograph of sample R3C. (bar = 2 µm).

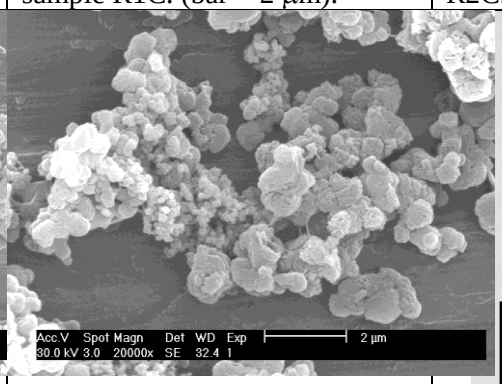

Figure 7. Micrograph of sample R4C. (bar = 2 µm).

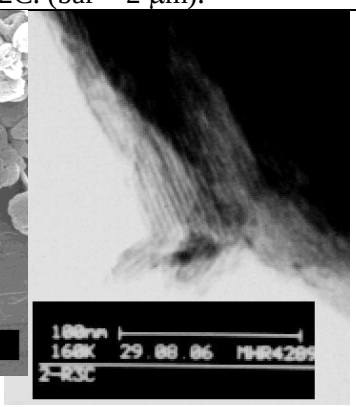

Figure 8. Micrograph TEM of sample R3C. (bar = 100 nm).

Figure 9 presents the thermogravimetric analysis of the samples T1, T2, T3 and T4. DTG analyzes (not presented here) helped to determine the temperature ranges for each event. For all exchanged samples we have the mass loss related to physisorbed water (A, $T < 130$ °C), the degradation of the organic cation, singular to each sample (B, $130 < T < 375$ °C) and the burning of residues and silicate dehydroxylation (C, $T > 375$ °C). Table 2 shows the total mass loss and, after discounting the physisorbed water, corresponds to organic compounds located at ion exchange sites. In terms of percentual mass loss, it was observed that these compounds correspond to losses between 9.7 and 12.4% of the total sample mass. However, we have that the number of percentual moles in these losses increases with the decreasing volume of the exchanged cation ($TBA^+ < TPA^+ < TEA^+ < TMA^+$). This behavior has two aspects: a) the *steric constraint*: bulky cations cannot be allocated on the surface of Nb-MCM-41 as much as the less bulky cations. When there are neighboring or nearby ion exchangeable sites, less bulky cations are better allocated among the sites, whereas bulky cations do not allow an adequate accommodation on the surface because they have kinetic diameter larger than the distance between two negative charges generated on the surface by the incorporation of Nb in the MCM-41 framework. Thus, the number of moles of exchanged cations should diminish when their volume increases; b) the *charge distribution on the organic cation*: the alkyl radicals are known electron donors and can assist in stabilizing the

central positive nitrogen of the organic cation. Increasing the size of this radical, increases the stabilizing effect, i.e., bulky cations have their charge distributed in a larger volume, decreasing the positive charge density, decreasing the basic character and are therefore less likely to perform ion exchange. Martins et al. (2008) observed similar behavior when carrying out the ionic exchange of alkylammonium cations with different volumes on zeolites X and Y.

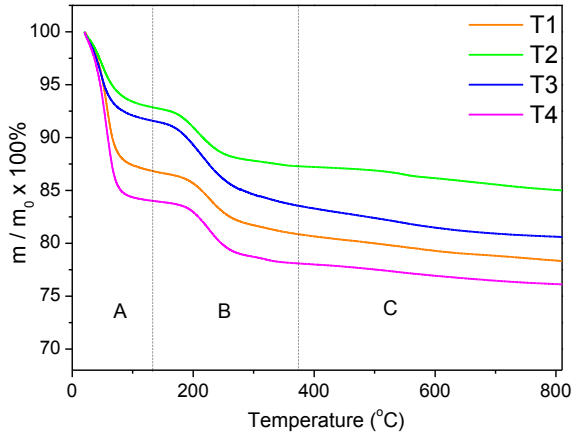

Figure 9. Thermogravimetric analyzes of the samples R1, R2, R3 and R4.

Table 2. Thermogravimetric Analyses in dry basis of the exchanged samples T1, T2, T3 e T4.

Temperature Range (ºC)	Event	Dry Basis			
		Mass Loss (%)			
		T1	T2	T3	T4
(B) 130 - 300 ºC	Template degradation	6	5,5	7,7	6,3
(C) > 300 ºC	Template burn and desidroxilation	4,3	3,7	4,6	3,6
Total loss (%m)	-	10,3	9,7	12,4	9,9
Organics loss (%molar)		0,138	0,074	0,067	0,041

Figure 10 presents the thermogravimetric analysis of the samples R1, R2, R3 and R4. For all recrystallized samples we have the mass loss related to physisorbed water (A, T < 130 °C), the glycerol decomposition (B, 105 < T < 210 °C), the organic cation decomposition, singular for each sample (C, 210 < T < 450 °C) and the burn of residues and silicate desidroxilation (D, T > 450 °C). Table 3 presents the total mass loss, after discounting the physisorbed water and glycerol, we have the organic compounds loss located at ion exchangeable sites. In terms of percentual mass loss it was observed that these compounds correspond to losses between 13 and 16.5% of the total mass sample. Here we have again that the number of percentual moles increases with decreasing the size of the exchange cation. This is expected because the recrystallization process tends to retain the exchanged cations on the surface and build microstructures templated by these cations.

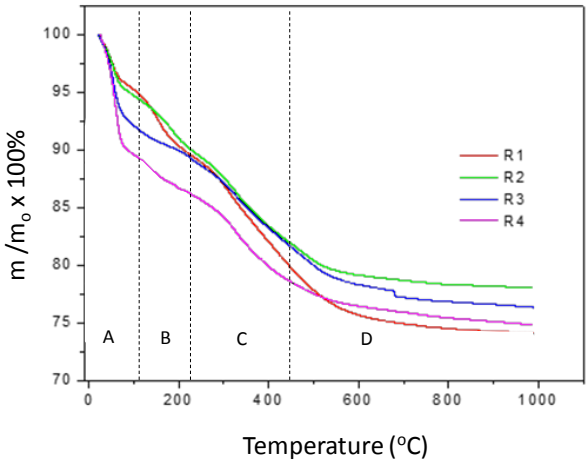

Figure 10. Thermogravimetric analyses for samples R1, R2, R3 e R4.

Tabela 3. Thermogravimetric analyses in dry basis for the recrystallized samples R1, R2, R3 e R4.

Temperature Range (ºC)	Event	Dry Basis			
		Mass Loss (%)			
		R1	R2	R3	R4
105 - 210 ºC	Glycerol decomposition	5,5	4,3	2,3	3,4
210 – 450 ºC	Organics decomposition	10,8	9,2	9	8,9
> 450 ºC	Desidroxilation	5,7	4	5,6	4,1
Total loss (%m)	-	16,5	13,2	14,6	13
Organics loss (%molar)		0,145	0,071	0,048	0,037

Figure 11 presents the N_2 physisorption isotherms for the matrix M and micro-mesostructured materials, RnC. The sample M presents a physisorption isotherm similar to Type II, according to the classification of De Boer et al. (1965), and typical for non-porous solids. The other isotherms, and especially MC (calcined matrix), are of type IV according to the this classification, and are typical for mesoporous materials. The recrystallized samples RnC present isotherms with increasing volumes of N_2 physisorbed from R1C to R4C samples. This means that the adsorbed volume increases by increasing the radius of the organic cation used in recrystallization ($TMA^+ < TEA^+ < TPA^+ < TBA^+$). The hysteresis aren't well defined, but could be classified as type A of the De Boer classification, or intermediate between H1 and H2 types proposed

by Sing (1968). However, with these data, it couldn't be possible to find evidence of the formation of micropores.

Thus, since the process for the preparation of hybrid materials was the same for all cases, it can be concluded that the bigger the cation used, better will be the preservation of the mesoporous structure. The amount of micropores possibly formed is very small and require the application of very low P/P0 to detect their presence and a long time of analysis, which was not possible with the standard physisorption equipment employed here.

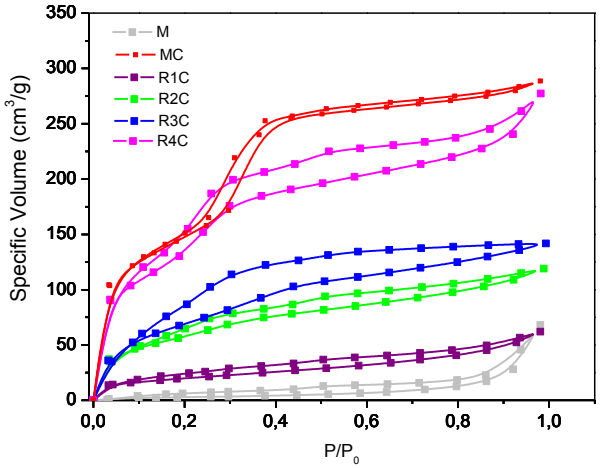

Figure 11. N_2 physisorption isotherms for the samples M, MC, R1C, R2C, R3C e R4C.

According to several authors and resumed by Gomes (2005), the niobium coordination can present four types of UV-vis bands: *band (I)*: $200 < \lambda < 235$ nm, related to structural tetrahedral niobium; *band (II)*: $245 < \lambda < 250$ nm, related to tetrahedral niobium distorted and hydrated; *band (III)*: around 270 nm, related to extra-structural niobia nanoparticles or Nb-O-Nb sites that interact with silicic surface; *band (IV)*: $260 < \lambda < 410$ nm, related to pure niobia. Figure 12 presents the UV-vis spectra for materials M, MC and RnC. We can observe a wide band centered at 245 nm for all samples, i.e., much of the Nb is in distorted tetrahedral arrangement, but bands (II) and (III) are present too, obliterated by the whole band. It wasn't observed pure niobia species.

Analyzing the calcined samples, we observed that the amount of tetrahedral distorted increases in the order MC~ R4C < R3C < R2C, except to R1C. The TBA^+ cation seems not to interfere in the Nb distorted tetrahedral coordination. As they are bulky cations, and since they are in small amounts on the surface of Nb-MCM-41, its presence has only to compensate sites easily accessible and whose steric constraint allows exchange without necessarily inducing a change in coordination. Decreasing the cation volume, Nb sites that in the previous situation would not be accessible to ion exchange, are induced to tetrahedral coordination, increasing its quantity and accommodating these cations. Possibly the increasing of charge density when decreasing the volume of the organic cation induces Nb sites to modify their coordination to receive these new charge compensators. The TMA^+ cation, the less bulky of all, should not induce only the change in the coordination of Nb sites because they easily become lodged around it, occupying positions in which water molecules would be allocated in distorted tetrahedral system.

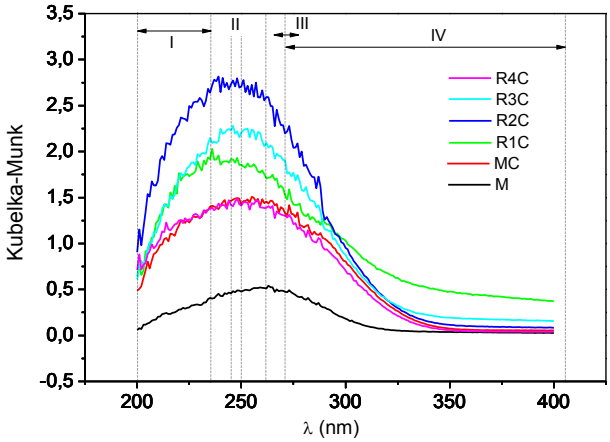

Figure 12. UV-vis spectra for M, MC and RnC.

4. CONCLUSIONS

The prepared composites maintained the mesoporous structure, but it was not possible to prove the formation of microporous structures by XRD or N_2 physisorption. However, the alkylammonium cations were retained on the solid in ion exchange sites before and after the recrystallization, which allows to infer the formation of microporous structures on the surface of the channels. The ion exchange method used for the synthesis of micro-mesostructured composites from Nb-MCM-41 matrix was efficient as the mesoporous structure was maintained in the final materials, as shown by X-ray diffraction. This is a unique aspect of this work.

Bulky cations are exchanged on the surface in smaller quantities than small cations. This is related to the steric constraints and to the charge density of these cations.

Niobium is inserted in the walls of the

mesoporous structure phase mainly in a distorted tetrahedral arrangement. This coordination is modified by surface exchanged cations which induce tetrahedral as its size decreases. For the TMA^+ cation, due to its smaller volume, this effect is less induced and possibly it allocates at hydration water positions.

5. ACKNOWLEDGEMENTS

To FAPESP (Fundação de Amparo à Pesquisa – SP), to the Dept. Chemical Engineering. and Dept. Materials Engineering (UFSCAR).

6. REFERENCES

BECK, J. S.; VARTULLI, J.C. et alii. A new family of mesoporous molecular sieves prepared with liquid crystal templating. *J. Am. Chem. Soc.*, v. 114, p. 10834 – 10843, 1992.

BORDOLOI, A.; DEVASSY, B. M.; NIPHADKAR, P. S.; JOSHI, P. N.; HALLIGUDI, S. B. Shape selective synthesis of long-chain linear alkylbenzene (LAB) with AlMCM-41/Beta zeolite composite catalyst. *J. Mol. Cat. A: Chem.*, v. 253, p. 239-244, 2006.

BURCHART, E. V.; KONINGSVELD, H. V.; GRAAF, B. V. Molecular mechanics studies of TBA and TPA in MEL and MFI. *Microporous Materials*, v. 8, p. 215-222, 1997.

CAI, Q.; LIN, W-Y.; XIAO, F.-S.; PANG, W-Q.; CHEN, X.-H.; ZOU, B.-S. The preparation of highly ordered MCM-41 with extremely low surfactant concentration. *Microp.Mesop. Mat.*, v. 32, p. 1-15, 1999.

CHENG, C.-F.; HO, D.; KLINOWSKI, J. Optimal parameters for the synthesis of the mesoporous molecular sieve [Si]-MCM-41. *J. Chem. Soc. – Faraday Trans.*, v. 93, n. 1, p. 193-197, 1997.

COPPENS, M.-C.; SUN, J.; MASHMEYER,T. Synthesis of hierarquical porous silicas with a controlled pore size distribution at various length scales. *Catal. Today*, v. 69, p. 331 – 335, 2001.

DE BOER, J.H.; LINSEN, B.G.; OSINGA, T.J. Studies on pore systems in catalysts. 6. Universal T curve. *J. Catal.*, v. 4, n. 6, p. 643, 1965.

GOMES, E.L. Síntese de peneiras moleculares contendo nióbio ou titânio e aplicação em epoxidação catalítica. Tese de Doutorado, UFSCar, São Carlos, Brasil, 376 f, 2005.

GOPAL, S.; YOO, K.; SMIRNIOTIS, P. G. Synthesis of Al-rich ZSM-12 using TEAOH as template. *Microp. Mesop. Mater.*, v.49, p. 149-156, 2001.

HUANG, L.; GUO, W.; DENG, P.; XUE, Z.; LI, Q. Investigation of synthesizing MCM 41 / ZSM 5 composites. *J. Phys. Chem. B*, v. 104, p. 2817 – 2823, 2000.

JAFARI, M; NOURI, A.;KAZEMIMOGHADAM, M.; MOHAMMADI, T. Investigations on hydrothermal synthesis parameters in preparation of nanoparticles of LTA zeolite with the aid of TMAOH. *Powder Technology*, v.237, p. 442–449, 2013.

PUSPARATU, Y. H. et alii. Isomerization and Cracking of Hexane over Beta Zeolites Synthesized by Dry Gel Conversion Method. *J. Japan Petr. Inst.*, v.55, n.2, p. 120-131, 2012.

GUALTIERI, M. L.; GUALTIERI, A. F.; HEDLUND, J. The influence of heating rate on template removal in silicalite-1: An in situ HT-XRPD study. *Microp. Mesop. Mat.*, v. 89, p. 1-8, 2006.

KLOETSTRA, K.R.; VAN BEKKUM, H.; JANSEN, J.C. Mesoporous material containing framework tectosilicate by pore-wall recrystallization. *Chem. Comm.*, p. 2281 – 2282, 1997.

MARTINS, L.; VIEIRA, K.M.; RIOS, L.M.; CARDOSO, D. Basic catalyzed Knoevenagel condensation by FAU zeolites exchanged with alkylammonium cations. *Catalysis Today*, v. 133–135, p. 706–710, 2008.

OCCELLI, O.P. Effects of isomorphous substitution of Si with Ti and Zr in mesoporous silicates with the MCM-41 structure. *Appl. Catal. A: General*, v. 183, p. 231-239, 1999.

ON, D.T.; KALIAGUINE, S. Large-pore mesoporous materials with semi-crystalline zeolítica frameworks. *Angew. Chem. Int. Ed.*, v. 40, n. 17, p. 3248 – 3251, 2001.

SING, K.S.W. Empirical method for analysis of adsoption isotherms. *Chem. Ind.*, v. 44, p. 1520, 1968.

WANG, S.; SHI, Y.; MA, X. GONG, J. Tuning Porosity of Ti-MCM-41: Implication for Shape Selective Catalysis. *ACS Appl. Mater. Interfaces*, v. 3, p. 2154–2160, 2011.

ZIOLEK, M. Niobium-containing catalysts – the state of the art. Catal. Today, v. 78, p. 47 – 64, 2003.